Nuclear Science and Techniques (2023) 34:70
https://doi.org/10.1007/s41365-023-01216-0

Assembly-level analysis on temperature coefficient of reactivity in a graphite-moderated fuel salt reactor fueled with low-enriched uranium

Xiao-Xiao Li[1,2,3] · De-Yang Cui[1,2] · Chun-Yan Zou[1,2,3] · Jian-Hui Wu[1,2,3] · Xiang-Zhou Cai[1,2,3] · Jin-Gen Chen[1,2,3]

Received: 29 November 2022 / Revised: 31 January 2023 / Accepted: 1 March 2023 / Published online: 16 May 2023

Abstract

To provide a reliable and comprehensive data reference for core geometry design of graphite-moderated and low-enriched uranium fueled molten salt reactors, the influences of geometric parameters on the temperature coefficient of reactivity (TCR) at an assembly level were characterized. A four-factor formula was introduced to explain how different reactivity coefficients behave in terms of the fuel salt volume fraction and assembly size. The results show that the fuel salt temperature coefficient (FSTC) is always negative owing to a more negative fuel salt density coefficient in the over-moderated region or a more negative Doppler coefficient in the under-moderated region. Depending on the fuel salt channel spacing, the graphite moderator temperature coefficient (MTC) can be negative or positive. Furthermore, an assembly with a smaller fuel salt channel spacing is more likely to exhibit a negative MTC. As the fuel salt volume fraction increases, the negative FSTC first weakens and then increases, owing to the fuel salt density effect gradually weakening from negative to positive feedback and then decreasing. Meanwhile, the MTC weakens as the thermal utilization coefficient caused by the graphite temperature effect deteriorates. Thus, the negative TCR first weakens and then strengthens, mainly because of the change in the fuel salt density coefficient. As the assembly size increases, the magnitude of the FSTC decreases monotonously owing to a monotonously weakened fuel salt Doppler coefficient, whereas the MTC changes from gradually weakened negative feedback to gradually enhanced positive feedback. Then, the negative TCR weakens. Therefore, to achieve a proper negative TCR, particularly a negative MTC, an assembly with a smaller fuel salt channel spacing in the under-moderated region is strongly recommended.

Keywords Molten salt reactor · Temperature coefficient of reactivity · Four-factor formula

This work was supported by the Youth Innovation Promotion Association CAS (No. 2022258), the National Natural Science Foundation of China (No. 12175300), the Chinese TMSR Strategic Pioneer Science and Technology Project (No. XDA02010000), and the Young Potential Program of Shanghai Institute of Applied Physics, Chinese Academy of Sciences (No. E1550510).

The original article has been updated: Due to Figure 5 update.

✉ Xiang-Zhou Cai
caixz@sinap.ac.cn

✉ Jin-Gen Chen
chenjg@sinap.ac.cn

[1] Shanghai Institute of Applied Physics, Chinese Academy of Sciences, Shanghai 201800, China

[2] CAS Innovative Academy in TMSR Energy System, Chinese Academy of Sciences, Shanghai 201800, China

[3] University of Chinese Academy of Sciences, Beijing 100049, China

Abbreviations

TCR	Temperature coefficient of reactivity
FSTC	Fuel salt temperature coefficient
MTC	Moderator temperature coefficient
VF	Fuel salt volume fraction
L	Assembly size
k_{inf}	Infinite multiplication factor
ε	Fast fission factor
p	Resonance escape probability
η	Thermal reproduction factor
f	Thermal utilization factor
A_1^{salt}	Thermal absorption of fuel salt
A_1^{gra}	Thermal absorption of graphite moderator
A_1^{HM}	Thermal absorption of heavy metal
A_1^{FLiBe}	Thermal absorption of carrier salt
$A_1^{\mathrm{FLiBe,gra}}$	Thermal absorption of carrier salt and graphite moderator

A_1^{tot}	Thermal absorption of all materials in the assembly
α_T(Salt)	Symbol for FSTC
α_T(Gra)	Symbol for MTC
α_T(Dop)	Symbol for Doppler coefficient
α_T(Den)	Symbol for density coefficient
α_T	Symbol for TCR
α_T^{ε}	Fast fission coefficient
α_T^{p}	Resonance escape coefficient
α_T^{η}	Thermal reproduction coefficient
α_T^{f}	Thermal utilization coefficient
EALF	Energy of average lethargy of fission
HM	Heavy metal
α_T^{ε}(Dop)	Fast fission coefficient in Doppler coefficient
α_T^{p}(Dop)	Resonance escape coefficient in Doppler coefficient
α_T^{η}(Dop)	Thermal reproduction coefficient in Doppler coefficient
α_T^{f}(Dop)	Thermal utilization coefficient in Doppler coefficient
α_T^{ε}(Den)	Fast fission coefficient in density coefficient
α_T^{p}(Den)	Resonance escape coefficient in density coefficient
α_T^{η}(Den)	Thermal reproduction coefficient in density coefficient
α_T^{f}(Den)	Thermal utilization coefficient in density coefficient
α_T^{ε}(Salt)	Fast fission coefficient in FSTC
α_T^{p}(Salt)	Resonance escape coefficient in FSTC
α_T^{η}(Salt)	Thermal reproduction coefficient in FSTC
α_T^{f}(Salt)	Thermal utilization coefficient in FSTC
α_T^{ε}(Gra)	Fast fission coefficient in MTC
α_T^{p}(Gra)	Resonance escape coefficient in MTC
α_T^{η}(Gra)	Thermal reproduction coefficient in MTC
α_T^{f}(Gra)	Thermal utilization coefficient in MTC
α_T^{ε}(Tot)	Fast fission coefficient in TCR
α_T^{p}(Tot)	Resonance escape coefficient in TCR
α_T^{η}(Tot)	Thermal reproduction coefficient in TCR
α_T^{f}(Tot)	Thermal utilization coefficient in TCR

1 Introduction

The molten salt reactor (MSR) is the only liquid-fueled reactor in the generation of IV power systems [1]. The core structure and operation mode of MSR are distinct from those of pressurized water reactors (PWR). A typical PWR uses water as the coolant and moderator. As the core temperature of a PWR increases, the water density decreases and the ratio of water to uranium declines, however, the fuel density remains almost constant. PWR is typically designed in the under-moderated region to ensure a sufficiently negative moderator temperature coefficient [2, 3]. A typical graphite-moderated MSR uses flowing fuel salt as the coolant and solid graphite as the moderator [4]. As the core temperature of an MSR increases, the density of the graphite moderator remains unchanged, while the density of the liquid fuel salt decreases, resulting in a higher ratio of graphite to nuclear fuel [5] and then significantly effects the temperature coefficient of reactivity (TCR). To make a reactor self-stable, it is crucial to maintain a proper negative temperature coefficient of reactivity (TCR) by adopting appropriate design parameters.

The TCR of a graphite-moderated and liquid-fueled MSR is typically divided into the fuel salt temperature coefficient (FSTC) and graphite moderator temperature coefficient (MTC). The FSTC is typically negative, which can be further divided into the fuel salt Doppler and fuel salt density coefficients [6]. However, the MTC can be negative or positive [7–9], and the positive MTC poses a potential safety risk to reactor operation. Currently, most liquid-fueled MSRs, such as MSRE [10], MSBR [11], and FUJI [12], are designed in the under-moderated region. Nevertheless, these designs did not provide a systematic analysis to explain why the under-moderated region was selected.

Some research has been conducted on the influencing factors of TCR in liquid-fueled MSRs, focusing on the geometric parameters and fuel salt compositions. The geometric parameters [13–15] include the fuel salt channel radius, fuel salt fraction, and lattice pitch. The molar ratio of heavy metals (HMs), type of carrier salt [16, 17], and uranium enrichment are all important parameters associated with fuel salt compositions. The effects of fuel salt composition on TCR for MSR have been studied using the six-factor formula [18–20]. However, further research is necessary to determine how geometric parameters affect TCR in an MSR core.

Based on a graphite-moderated and low-enriched uranium-fueled MSR, this study aimed to provide a more responsible contribution to variations of various reactivity coefficients with geometric parameters, including fuel salt volume fraction and assembly size. The remainder of this paper is organized as follows. Section 2 provides a brief overview of the calculation model and analysis methodology. Section 3 discusses the behavior of various reactivity coefficients from the perspective of the four-factor formula. Section 4 contains concluding remarks on TCR for liquid-fueled MSRs.

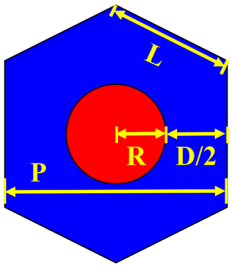

Fig. 1 Schematic of a graphite-moderated fuel salt assembly

2 Calculation model and analysis methodology

2.1 Calculation model

A graphite-moderated fuel salt assembly includes two regions (Fig. 1): a central circular region filled with fuel salt (defined as the fuel salt channel) and a hexagonal outer region comprising a graphite moderator. The assembly geometry can be characterized by the side length of the assembly (L), the opposite side distance (P), the radius of the fuel salt channel (R), and the fuel salt channel spacing (D), representing the distance between two adjacent fuel salt channels' outer margins. Notably, the maximum fuel salt volume fraction (VF) was set to 50%. This is primarily because there is almost no Maxwell spectrum and MTC approaches zero when the fuel salt volume fraction exceeds 50%.

The adopted fuel salt composition in this study is LiF-BeF_2-UF_4 (68-20-12 mole%). Previous studies have revealed more detailed analyses of the effect of the concentration of HMs on TCR [18, 19], which will not be discussed in this work. To reduce the harmful neutron absorption of Li-6, the abundance of Li-7 was set to 99.995%. Low enriched uranium (< 20% U-235 enrichment) was used in this study for nonproliferation and availability.

2.2 Analysis methodology

This study was conducted for a single graphite-moderated fuel salt assembly that was infinitely reflected in both the radial and axial directions. In this case, the moderator is graphite, and the nuclear fuel melted in the carrier salt [21, 22], which includes F, Li, and Be and exhibits certain moderating properties [23, 24]. The four-factor formula for an infinite medium [25, 26], $k_{\mathrm{inf}} = \varepsilon p \eta f$, is used to qualitatively elucidate the mechanisms of TCR of an MSR at the assembly level. Here, ε, p, η, and f represent the fast fission factor, resonance escape probability, thermal reproduction factor, and thermal utilization factor, respectively. The four factors and their corresponding reactivity coefficients for a graphite-moderated fuel-salt assembly with low-enriched uranium are detailed as follows. It is crucial to consider that nuclear fuels (or HMs) are integrated into the fuel salt, and their fission or absorption contributions should be subtracted from the fuel salt when calculating the four factors, particularly for the fast fission and thermal reproduction factors.

The fast fission factor $\varepsilon = F_{\mathrm{t}}^{\mathrm{HM}}/F_{\mathrm{l}}^{\mathrm{HM}}$ is defined as the ratio of the number of neutrons produced by fissions at all energies (total production) to that produced by thermal fission (thermal production). The thermal reproduction factor $\eta = F_{\mathrm{l}}^{\mathrm{HM}}/A_{\mathrm{l}}^{\mathrm{HM}}$ is the ratio of the number of neutrons produced by thermal fission (thermal production) to that of thermal neutrons absorbed in nuclear fuel (thermal absorption). Here, F_{t}, F_{l}, and A_{l} represent the total production, thermal production, and thermal absorption, respectively. Because fast fission occurs primarily in U-238 but also in U-235 when low-enriched uranium is used, the subscript "HM" includes U-235 and U-238.

The resonance escape probability, $p = A_{\mathrm{l}}^{\mathrm{tot}}/A_{t}^{\mathrm{tot}} = A_{\mathrm{l}}^{\mathrm{salt}} + A_{\mathrm{l}}^{\mathrm{gra}}$, is described as the ratio of neutrons reaching thermal energies to fast neutrons slowing. The thermal utilization factor, $f = A_{\mathrm{l}}^{\mathrm{HM}}/A_{\mathrm{l}}^{\mathrm{tot}} = A_{\mathrm{l}}^{\mathrm{HM}}/(A_{\mathrm{l}}^{\mathrm{HM}} + A_{\mathrm{l}}^{\mathrm{FLiBe}} + A_{\mathrm{l}}^{\mathrm{gra}}) = A_{\mathrm{l}}^{\mathrm{HM}}/(A_{\mathrm{l}}^{\mathrm{HM}} + A_{\mathrm{l}}^{\mathrm{FLiBe,gra}})$, is represented as the ratio of the thermal neutrons absorbed in the HM to those absorbed in all the materials in the assembly. Here, A_{t} represents the total absorption, and $A_{\mathrm{t}}^{\mathrm{tot}}$ equals 1.0. The superscripts "HM," "FLiBe," "gra," and "tot" represent the thermal absorption of HMs, carrier salt, graphite, and all the materials in the assembly, respectively.

The temperature coefficient of reactivity, α_{T}, defined as the change in reactivity caused by the change in temperature of all materials in the assembly [27], is expressed by Eq. (1) when k_{inf} approaches 1.0. The temperature (T) increases in 100 K increments from 780 K to 1080 K, considering the melting point of the fuel salt and the possible temperature range of MSR.

$$\alpha_{\mathrm{T}} = \frac{1}{k_{\mathrm{inf}}}\frac{\mathrm{d}k_{\mathrm{inf}}}{\mathrm{d}T} \tag{1}$$

According to Eq. (2), each TCR can be decomposed into four reactivity coefficients [28]: the fast fission ($\alpha_{\mathrm{T}}^{\varepsilon}$), resonance escape ($\alpha_{\mathrm{T}}^{p}$), thermal reproduction ($\alpha_{\mathrm{T}}^{\eta}$), and thermal utilization (α_{T}^{f}).

$$\alpha_{\mathrm{T}} = \alpha_{\mathrm{T}}^{\varepsilon} + \alpha_{\mathrm{T}}^{p} + \alpha_{\mathrm{T}}^{\eta} + \alpha_{\mathrm{T}}^{f} \tag{2}$$

Equations (3)–(6) presents the calculation methods for the four reactivity coefficients. Here, "d" denotes the absolute change in parameter caused by temperature change and "Δ" denotes the rate at which the parameter changes with temperature.

$$\alpha_{\mathrm{T}}^{\varepsilon}=\frac{1}{\varepsilon}\frac{\mathrm{d}\varepsilon}{\mathrm{d}T}=\Delta F_{\mathrm{t}}^{\mathrm{HM}}-\Delta F_{1}^{\mathrm{HM}}= \frac{1}{F_{\mathrm{t}}^{\mathrm{HM}}}\frac{\mathrm{d}F_{\mathrm{t}}^{\mathrm{HM}}}{\mathrm{d}T}-\frac{1}{F_{1}^{\mathrm{HM}}}\frac{\mathrm{d}F_{1}^{\mathrm{HM}}}{\mathrm{d}T} \tag{3}$$

$$\alpha_{\mathrm{T}}^{p}=\frac{1}{p}\frac{\mathrm{d}p}{\mathrm{d}T}=\Delta A_{1}^{\mathrm{salt}}+\Delta A_{1}^{\mathrm{gra}}= \frac{1}{A_{1}^{\mathrm{salt}}+A_{1}^{\mathrm{gra}}}\left(\frac{\mathrm{d}A_{1}^{\mathrm{salt}}}{\mathrm{d}T}+\frac{\mathrm{d}A_{1}^{\mathrm{gra}}}{\mathrm{d}T}\right) \tag{4}$$

$$\alpha_{\mathrm{T}}^{\eta}=\frac{1}{\eta}\frac{\mathrm{d}\eta}{\mathrm{d}T}=\Delta F_{1}^{\mathrm{HM}}-\Delta A_{1}^{\mathrm{HM}} =\frac{1}{F_{1}^{\mathrm{HM}}}\frac{\mathrm{d}F_{1}^{\mathrm{HM}}}{\mathrm{d}T}-\frac{1}{A_{1}^{\mathrm{HM}}}\frac{\mathrm{d}A_{1}^{\mathrm{HM}}}{\mathrm{d}T} \tag{5}$$

$$\alpha_{\mathrm{T}}^{f}=\frac{1}{f}\frac{\mathrm{d}f}{\mathrm{d}T}=\Delta A_{1}^{\mathrm{HM}}-\Delta A_{1}^{\mathrm{FLiBe,gra}} =\frac{A_{1}^{\mathrm{FLiBe,gra}}}{A_{1}^{\mathrm{tot}}}\left(\frac{1}{A_{1}^{\mathrm{HM}}}\frac{\mathrm{d}A_{1}^{\mathrm{HM}}}{\mathrm{d}T}-\frac{1}{A_{1}^{\mathrm{FLiBe,gra}}}\frac{\mathrm{d}A_{1}^{\mathrm{FLiBe,gra}}}{\mathrm{d}T}\right) \tag{6}$$

Notably, U-235 plays a dominate role in feedback, particularly for $\alpha_{\mathrm{T}}^{\varepsilon}$ and $\alpha_{\mathrm{T}}^{\eta}$, because its microscopic cross section is significantly higher than that of U-238 over the thermal energy region, particularly when neutron energy is < 0.1 eV. Therefore, in the following discussion, we focus on U-235's contribution to the fast fission ($\alpha_{\mathrm{T}}^{\varepsilon}$) and thermal reproduction coefficients ($\alpha_{\mathrm{T}}^{\eta}$).

MCNP5 handles neutronic calculations, such as criticality and reactivity coefficients. The FMn tally multiplier card is used to calculate the cross sections and factors in the four-factor formula. To perform accurate calculations with uranium-based fuel, a compact ENDF (ACE) format cross-section library with continuous energy was selected based on the ENDF/B-VII library. To increase computational accuracy and efficiency, each criticality calculation is excused to skip 50 cycles and run 1050 cycles with 100,000 neutrons per cycle. The maximum computing time for one criticality calculation using 12 processors was < 36 h. The estimated standard deviation of k_{inf} is approximately 5 pcm.

3 Results and discussions

3.1 Critical parameters

Considering the characteristics of online refueling and reprocessing for a liquid-fueled MSR, the initial excess reactivity of a graphite-moderated fuel salt assembly can be set as low (k_{inf} = 1.02~1.03). Then, the required critical enrichment

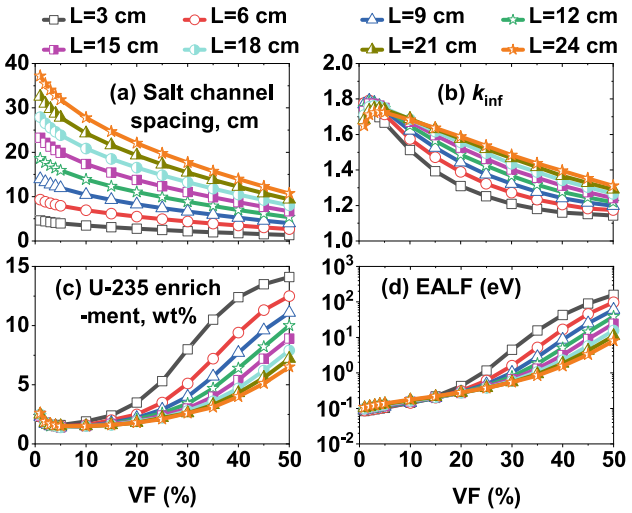

Fig. 2 (Color online) Variations of fuel salt channel spacing (**a**), k_{inf} (**b**), critical enrichment of U-235 (**c**) and EALF (**d**) with fuel salt volume fraction for different assembly sizes

of U-235 was searched by varying assembly size (L) from 3.0 to 24.0 cm and fuel salt VF from 1 to 50%. The fuel salt channel spacing is closely related to the required critical enrichment of U-235 and the temperature coefficient of reactivity, and its variation with the fuel salt volume fraction and assembly size is shown in Fig. 2a. Increasing the fuel salt volume fraction and decreasing the assembly size can result in a decrease in the fuel salt channel spacing. Meanwhile, the larger the assembly size, the faster the fuel salt channel spacing decreases with increasing fuel salt volume fraction.

The variations in the infinite multiplication factor at a fixed U-235 enrichment (19.75 wt%) and the required critical enrichment of U-235 with fuel salt volume fraction and assembly size are given in Figs. 2b and c , respectively. When the fuel salt volume fraction is increased for a fixed assembly size, the neutron spectrum hardens, and the residence time of neutrons in the high-energy region of fast fission is prolonged. Hence, the fast neutron multiplication effect is enhanced, and the fast fission factor increases. Meanwhile, as the graphite moderator volume fraction decreases, the ratio of graphite to HM declines, and the probability of neutrons being absorbed by nuclear fuel or moderator in the epi-thermal neutron energy region increases, making it more difficult for neutrons to escape from the resonance region, and thus the resonance escape probability decreases. However, the thermal reproduction factor only varied slightly with the fuel salt volume fraction, with a maximum variation of < 0.6%. As the ratio of fuel salt volume to graphite volume further increased, the thermal absorption of the fuel salt exceeded that of graphite, and the thermal utilization factor increased. Based on the variations in the four factors, the infinite multiplication factor first

increased corresponding to the under-moderated region and then decreased corresponding to the over-moderated region as the fuel salt volume fraction increased. In contrast, the required critical enrichment of U-235 decreased in the over-moderated region and then increased in the under-moderated region.

For a constant fuel salt volume fraction, as the assembly size increased, the graphite through which the incident neutrons thicken, neutrons could be better slowed down, and the neutron spectrum softened. In this case, the fast neutron multiplication effect weakens, and the fast fission factor decreases. Meanwhile, the absorption probability of resonance neutrons generated in graphite by HMs decreases, resulting in an increase in resonance escape probability [29]. The thermal reproduction factor as also not visibly affected by the assembly size, with a maximum variation of $< 0.4\%$. As the fuel salt channel spacing increased with increasing assembly size, the thermal neutron absorption of nuclear fuel decreased while that of the graphite moderator increased, and then the thermal utilization factor decreased. As the assembly size increased, a slight decrement in the infinite multiplication factor and a slight increment in the required critical enrichment of U-235 were displayed in the over-moderated region. Meanwhile, the infinite multiplication factor increased, while the required critical enrichment of U-235 fell in the under-moderated region.

The neutron spectrum is essential for determining the factors influencing TCR. To quantitatively characterize the neutron spectrum in a reactor, a spectrum factor defined as the energy corresponding to the average neutron lethargy causing fission (EALF) [19] is introduced, and its variation with the fuel salt volume fraction and assembly size is displayed in Fig. 2d. As the fuel salt volume fraction increased for a constant assembly size, the required critical enrichment of U-235 increased, particularly in the under-moderated region, allowing for more production of fast neutrons. As the fuel salt channel spacing decreases, the fast neutrons released from the fuel salt cannot be fully moderated. These two factors harden the neutron spectrum, leading to an increase in EALF. The effect of the assembly size on the EALF is associated with the moderated region. First, when the assembly tends to the over-moderated region, the graphite parasitic absorption becomes stronger, and the likelihood of fast neutrons being slowed down to thermal neutrons decreases. In addition, a slight increase in the required critical enrichment of U-235 resulted in more fast neutron generation as the assembly size increased. Thus, the neutron spectrum hardens, and EALF increases as the assembly size increases in the over-moderated region. Second, when the assembly tends toward the under-moderated region, graphite dominates the scattering reaction. As the assembly size increases, the likelihood of fast neutrons colliding with graphite nuclides increases, along with the possibility of fast neutrons slowing down into thermal neutrons. Simultaneously, an increasing assembly size causes a decrease in the required critical enrichment of U-235 and less fast neutron generation. Thus, the neutron spectrum softens and the EALF decreases as the assembly size increases in the under-moderated region.

3.2 Fuel salt Doppler coefficient

The Doppler effect can be used to explain the Doppler broadening of the resonance capture cross sections of nuclear fuel because it determines the fuel salt temperature coefficient. From the point of view of the four-factor formula, the fuel salt Doppler coefficient can be decomposed into four reactivity coefficients, that is, the fast fission, resonance escape, thermal reproduction, and thermal utilization coefficients , as demonstrated in Eq. (2). Their variations with the fuel salt volume fraction and assembly size are presented in Fig. 3.

The Doppler broadening of resonance caused by an increase in fuel salt temperature leads to a hardening neutron spectrum, which causes the residence time of neutrons in the high-energy region of fast fission to be longer, the fast neutron multiplication effect to be enhanced, and the fast fission factor to increase. Thus, the fast fission coefficient in the Doppler coefficient, $\alpha_{\mathrm{T}}^{\varepsilon}(\mathrm{dop})$, is positive. Its magnitude is primarily determined by the difference between U-235's thermal and total productions, and it is very closely related to the change of the neutron spectrum. When the fuel salt volume fraction or assembly size changes, if the neutron spectrum becomes harder and EALF increases, the proportion of U-235's thermal production in U-235's total production decreases, and the gap between the variations in U-235's total and thermal productions widens. This implies that the magnitude of the fast fission coefficient in the Doppler coefficient increases. In contrast, when the neutron spectrum softens, the magnitude of the fast fission coefficient in the Doppler coefficient decreases. Consequently, Fig. 3a shows that for a constant assembly size, the magnitude of the fast fission coefficient in the Doppler coefficient increases monotonously as the fuel salt volume fraction increases. As the assembly size increases for a fixed fuel salt volume fraction, the magnitude of the fast fission coefficient in the Doppler coefficient increases slightly in the over-moderated region, but significantly decreases in the under-moderated region. Overall, the magnitude of the fast fission coefficient in the Doppler coefficient is positively correlated with the EALF.

When the fuel salt temperature increases, the Doppler broadening effect enhances the resonance absorption of nuclear fuel and lowers the likelihood of neutrons passing through the epi-thermal region to the thermal region, and the thermal absorption of fuel salt decreases. Nevertheless, the thermal absorption of graphite may decrease for a smaller fuel salt channel spacing or increase for a larger fuel salt

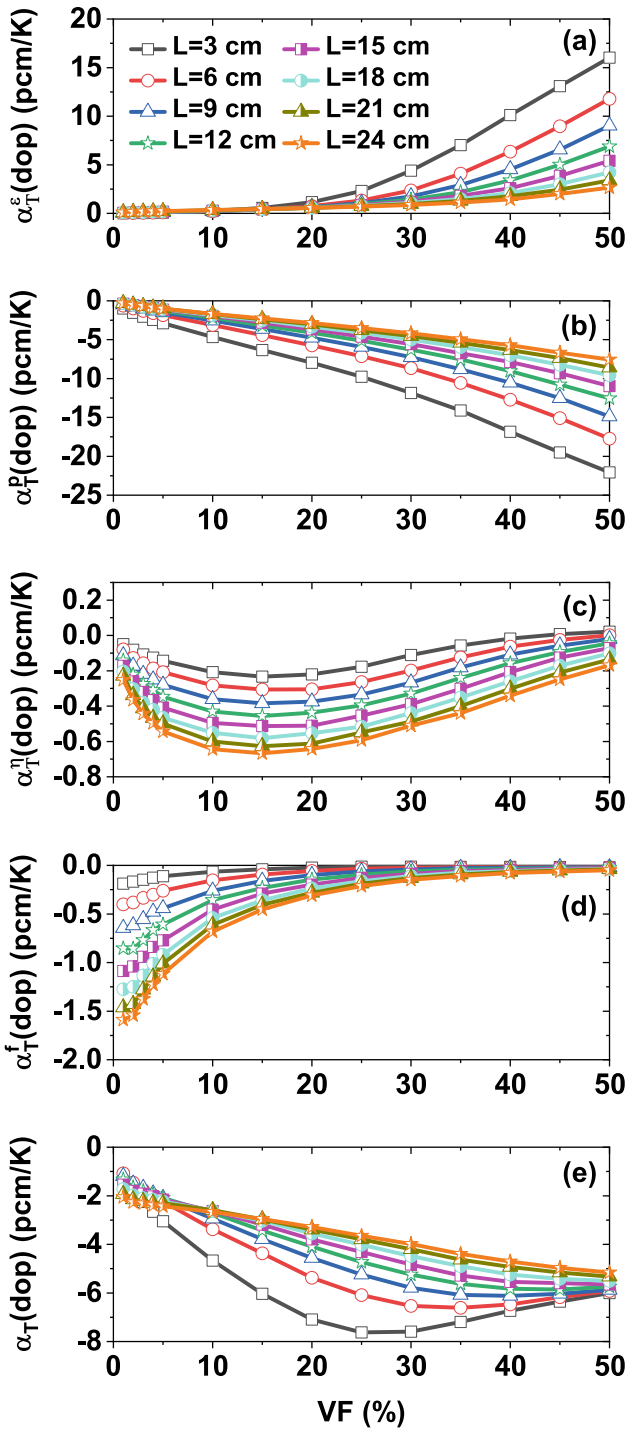

Fig. 3 (Color online) Variations in different reactivity coefficients caused by the Doppler effect with fuel salt volume fraction and assembly size. **a** α_T^{ε}(dop): fast fission coefficient in Doppler coefficient; **b** α_T^{p}(dop): resonance escape coefficient in Doppler coefficient; **c** α_T^{η}(dop): thermal reproduction coefficient in Doppler coefficient; **d** α_T^{f}(dop): thermal utilization coefficient in Doppler coefficient; and **e** α_T(dop): Doppler coefficient

channel spacing. This is because the thermal neutrons generated mainly in graphite have a higher probability of being absorbed by graphite itself when the fuel salt channel spacing is relatively large. Because the Doppler effect mainly affects the HMs in fuel salt, the change in thermal absorption of fuel salt is typically at least one order of magnitude greater than the change in thermal absorption of graphite. Thus, the sum of the changes in the thermal absorptions of the fuel salt and graphite is always negative. Consequently, the resonance escape coefficient in the Doppler coefficient, α_T^{p}(dop), is negative. Figure 3b shows that the variation in the resonance escape coefficient in the Doppler coefficient comes mainly from the sum of the thermal absorptions of the fuel salt and graphite, and to a lesser degree, from their changes. That is, for a constant assembly size, as the fuel salt volume fraction increases, a harder neutron spectrum lowers the sum of the thermal absorptions of fuel salt and graphite. Hence, a larger variation in the resonance escape probability is revealed, and a stronger resonance escape coefficient in the Doppler coefficient is presented for a larger fuel salt volume fraction corresponding to a smaller fuel salt channel spacing. As the assembly size increases for a fixed fuel salt volume fraction, the fuel salt channel spacing widens, and the sum of the thermal absorptions of the fuel salt and graphite gradually increases, weakening the resonance escape coefficient in the Doppler coefficient.

The Doppler broadening effect hardens the neutron spectrum, increasing the resonance absorption of nuclear fuel and decreasing the probability of thermal neutrons being absorbed by nuclear fuel. Both the thermal production and total absorption of U-235 decrease. Because the microscopic fission cross section of U-235 is greater than its microscopic capture cross section, particularly in the thermal neutron region, and the average number of fission neutrons of U-235 is generally > 2.0, the absolute decrement of thermal production is always stronger than that of thermal absorption. For most combinations of fuel salt volume fraction and assembly size, despite the fact that U-235's thermal production is larger than U-235's thermal absorption, the absolute variation in U-235's thermal production remains larger than that in U-235's thermal absorption, and then the thermal reproduction factor decreases and further leads to a negative thermal reproduction coefficient in the Doppler coefficient (α_T^{η}(dop)). However, for an assembly with a very small fuel salt channel spacing (e.g., $L = 3$ cm and $VF = 40\%$), the graphite thickness that neutrons pass is relatively small, neutrons are not sufficiently slowed down, and the probability of thermal neutron production is reduced, as is U-235's absorption (both fission and capture). In this case, the difference between U-235's thermal production and its thermal absorption is greater than the difference between the decrement of U-235's thermal production and that of U-235's thermal absorption. Thus, the variation in U-235's thermal

production has a lower absolute value than that of its thermal absorption, increasing the thermal reproduction factor and causing a positive thermal reproduction coefficient in the Doppler coefficient. Figure 3c shows that the magnitude of the thermal reproduction coefficient in the Doppler coefficient first increases and then decreases as the fuel salt volume fraction increases, but increases monotonously with increasing assembly size. First, as the fuel salt volume fraction increases, a hardening neutron spectrum causes decrements in both U-235's thermal production and its thermal absorption, followed by increments in both the variation in U-235's thermal production and that in its thermal absorption. When the fuel salt volume fraction begins to increase, the proportion of thermal neutrons is relatively high, and the increase in the variation in U-235's thermal production is greater than that in U-235's thermal absorption, causing the magnitude of the thermal reproduction coefficient in the Doppler coefficient to increase slightly. However, as the fuel salt volume fraction continues to increase, the share of thermal neutron absorption decreases, while the share of resonance neutron absorption and fast neutron absorption increases. At this point, the increase in the variation in U-235's thermal absorption gradually exceeds that in its thermal production, causing the magnitude of the thermal reproduction coefficient in the Doppler coefficient to decrease. The negative thermal reproduction coefficient in the Doppler coefficient first strengthens and then weakens as the fuel salt volume fraction increases for a constant assembly size. Second, the change in the thermal reproduction coefficient in the Doppler coefficient with assembly size is divided into two phases according to the fuel salt volume fraction. When the fuel salt volume fraction is very small (e.g., $VF = 1\%$) or very large (e.g., $VF = 40\%$), the absolute changes in U-235's thermal production and U-235's thermal absorption increase with increasing assembly size, however, the former increases faster than the latter. Consequently, the increment in the variation in U-235's thermal production is greater than that in U-235's thermal absorption, and the magnitude of the thermal reproduction coefficient in the Doppler coefficient increases as the assembly size increases. When the fuel salt volume fraction is close to the optimal moderated zone (e.g., $VF = 15\%$), an increasing resonance absorption share causes the absolute changes in U-235's thermal production and that of U-235's thermal absorption to decrease with increasing assembly size, with the latter decreasing faster than the former. The decrease in the variation in U-235's thermal absorption is greater than that in U-235's thermal production, and the magnitude of the thermal reproduction coefficient in the Doppler coefficient still increases as the assembly size increases. Therefore, when the fuel salt volume fraction is constant, the magnitude of the thermal reproduction coefficient in the Doppler coefficient increases monotonously with increasing assembly size. Notably, the magnitudes of the thermal reproduction coefficient in the Doppler coefficient for all combinations of fuel salt volume fraction and assembly size are small (< 0.7 pcm/K).

The thermal absorption of fuel salt decreases as the fuel salt temperature increases owing to a hardening neutron spectrum caused by the Doppler effect. Subsequently, the thermal absorptions of the HM and carrier salt decrease. The variation in the thermal absorption of graphite is related to the fuel salt channel spacing. First, for an assembly with a smaller fuel salt channel spacing, the thermal absorption of graphite is primarily affected by the hardening neutron spectrum, and the thermal absorption of graphite decreases, along with the sum of the thermal absorptions of the carrier salt and graphite. Second, as the fuel salt channel spacing increases, neutrons have more chances of colliding with graphite nuclei, the probability of neutrons slowing down into thermal neutrons increases, and the thermal absorption of graphite increases. In this case, the sum of the thermal absorptions of the carrier salt and graphite may increase in the over-moderated region or decrease in the under-moderated region. However, In either case, the change in the thermal absorption of HMs is always stronger than that in the sum of the thermal absorptions of the carrier salt and graphite caused by the Doppler effect, resulting in a decrease in the thermal utilization factor and a negative thermal utilization coefficient in the Doppler coefficient (α_{T}^{f} (dop)). The magnitude of the thermal utilization coefficient in the Doppler coefficient is primarily related to the ratio of the sum of the thermal absorptions of the carrier salt and graphite to the thermal absorptions of all materials, according to Eq. 6. From Fig. 3d, for a fixed assembly size, as the fuel salt volume fraction increases, the fuel salt channel spacing decreases, the graphite volume fraction decreases, and the ratio of the sum of the thermal absorptions of the carrier salt and graphite to the thermal absorptions of all materials is < 1.0 and becomes smaller, whereas the negative thermal utilization coefficient in the Doppler coefficient weakens. Meanwhile, for a constant fuel salt volume fraction, as the assembly size increases, the graphite thickness through which neutrons pass between two collisions with nuclear fuel increases, implying that more thermal neutrons may be absorbed by graphite. Then, the ratio of the sum of the thermal absorptions of the carrier salt and graphite to the thermal absorptions of all materials grows increasingly larger, and the negative thermal utilization coefficient in the Doppler coefficient strengths. To summarize, the negative thermal utilization coefficient in the Doppler coefficient is proportional to the fuel salt channel spacing.

Figure 3e depicts the variation in the Doppler coefficient with the fuel salt volume fraction and assembly size. The behavior of the Doppler coefficient is primarily governed by variations in the fast fission, resonance escape, and thermal

utilization coefficients. Because the sum of the negative resonance escape and negative thermal utilization coefficients is always greater than that of the positive fast fission coefficient, the Doppler coefficient is always negative. The magnitude of the Doppler coefficient varies with the fuel salt volume fraction, mainly depending on the competition between the fast fission and resonance escape coefficients. Increasing the fuel salt volume fraction increases the magnitude of the Doppler coefficient firstly due mainly to an enhancement in the resonance escape coefficient, and it reaches a maximum negative value before beginning to decrease with further increases in the fuel salt volume fraction owing to an enhancing positive fast fission coefficient. As the assembly size increases, the magnitude of the fuel salt Doppler coefficient increases in the over-moderated region owing to a slight enhancement in the thermal utilization coefficient and decreases in the under-moderated region owing to a gradually weakened resonance escape coefficient.

3.3 Fuel salt density coefficient

The fuel salt density effect occurs because a small amount of fuel salt is ejected from the reactor core as its density decreases with increasing fuel salt temperature. The decrease in fuel salt density results in two major effects: the first is an increase in collision probability between fast neutrons and graphite nuclei as a result of the reduced collision probability between fast neutrons and nuclear fuel, and the second is a reduction in resonance absorption of nuclear fuel, which results in more fast neutrons being slowed down to thermal neutrons. Both effects can soften the neutron spectrum and influence the fuel salt density coefficient. Similar to the fuel salt Doppler coefficient, the fuel salt density coefficient can also be divided into four parts: the fast fission, resonance escape, thermal reproduction, and thermal utilization coefficients caused by the fuel salt density effect. The variations in the fuel salt density coefficient and its four reactivity coefficients are presented in Fig. 4.

When the fuel salt temperature increases, a softening neutron spectrum caused by the fuel salt density effect weakens the fast neutron multiplication effect, and then the fast fission factor reduces. Thus, the fast fission coefficient in the density coefficient, α_T^{ε}(den), is negative. The variation in the fast fission coefficient in the density coefficient with the fuel salt volume fraction and assembly size is similar to that in the Doppler coefficient, and it is primarily determined by the shift of the neutron spectrum. As shown in Fig. 4a, for a constant assembly size, as the fuel salt volume fraction increases, the neutron spectrum hardens, the proportion of thermal production in the total production for U-235 decreases, the gap between the variation in U-235's total production and that in U-235's thermal production increases, and then the fast fission coefficient in the density coefficient

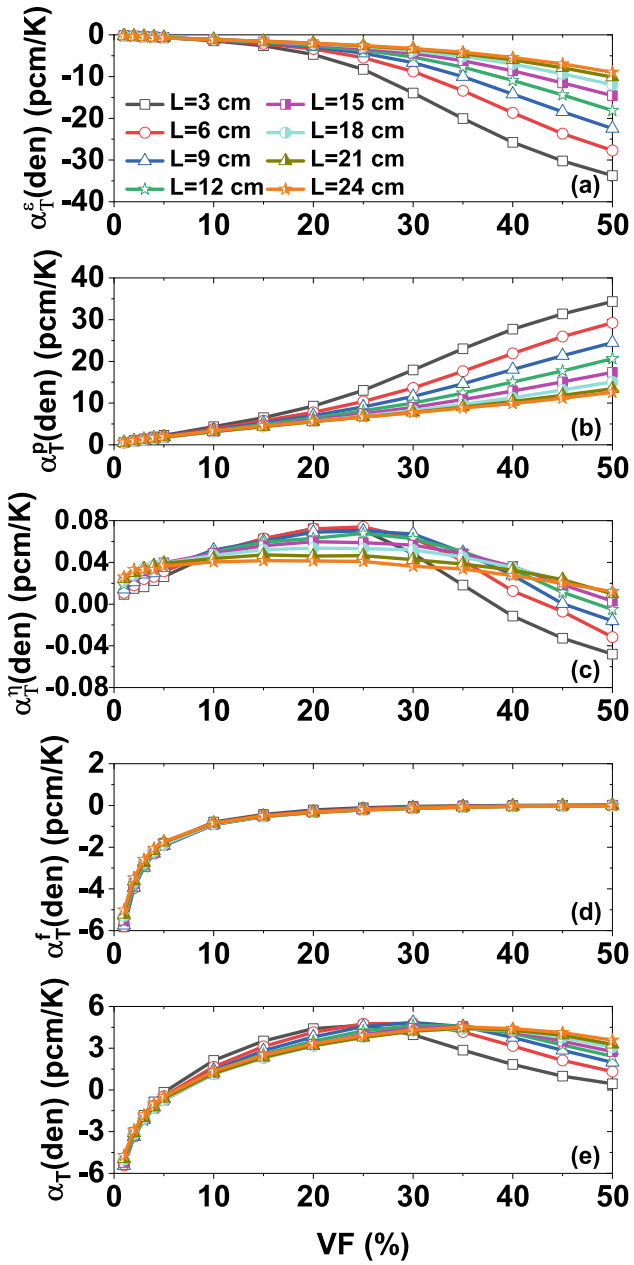

Fig. 4 (Color online) Variations in different reactivity coefficients caused by the fuel salt density effect with fuel salt volume fraction and assembly size. **a** α_T^{ε}(den): fast fission coefficient in density coefficient; **b** α_T^{p}(den): resonance escape coefficient in density coefficient; **c** α_T^{η}(den): thermal reproduction coefficient in density coefficient; **d** α_T^{f}(den): thermal utilization coefficient in density coefficient; and **e** α_T(den): density coefficient

is enhanced. Similarly, as the assembly size increases, the magnitude of the fast fission coefficient in the density coefficient either increases because of a gradual hardening neutron spectrum in the over-moderated region or decreases because of a gradual softening neutron spectrum in the under-moderated region. In general, the magnitude of the fast fission

coefficient in the density coefficient is positively correlated with the EALF.

As the fuel salt temperature increases, a softening neutron spectrum caused by the fuel salt density effect increases the thermal absorption of graphite. The change in the thermal absorption of fuel salt is influenced by both density reduction and spectrum softening, which is closely related to the moderated region. In the over-moderated region, the change in thermal absorption of fuel salt is mainly due to a decrease in fuel salt density, resulting in a numerical decrease. In this case, a lower fuel salt volume fraction corresponds to a higher graphite volume share, and the decrease in the thermal absorption of the fuel salt is smaller than the increase in the thermal absorption of graphite. Thus, the sum of the thermal absorptions of the fuel salt and graphite is positive. In the under-moderated region, the change in thermal absorption of fuel salt is primarily due to a softening neutron spectrum, and its value increases, along with the sum of the thermal absorptions of fuel salt and graphite. The resonance escape probability increases in either case, and the resonance escape coefficient in the density coefficient, $\alpha_{\mathrm{T}}^{p}(\mathrm{den})$, is positive. Figure 4b shows that the magnitude of the resonance escape coefficient in the density coefficient is also associated with the fuel salt channel spacing, and its variation with the fuel salt volume fraction and assembly size is determined by the sum of the thermal absorptions of the fuel salt and graphite. As the fuel salt volume fraction increases or the assembly size decreases, the sum of the thermal absorptions of the fuel salt and graphite increases, along with the magnitude of the resonance escape coefficient in the density coefficient. In short, the magnitude of the resonance escape coefficient in the density coefficient is inversely related to the fuel salt channel spacing.

The fuel salt density effect causes a decrease in the fuel salt density and a softening neutron spectrum as the fuel salt temperature increases. These two variables can determine whether the thermal reproduction coefficient in the density coefficient, $\alpha_{\mathrm{T}}^{\eta}(\mathrm{den})$, is positive or negative. First, the density reduction is typically reflected in the region with a relatively soft neutron spectrum (such as $VF = 1\%$). In this case, even though the decrement of U-235's thermal production is greater than that of U-235's thermal absorption, the decrement of the variation in U-235's thermal production is smaller than that in U-235's thermal absorption because U-235's thermal production is markedly greater than U-235's thermal absorption, and a positive thermal reproduction coefficient in the density coefficient is presented. Second, a softening neutron spectrum causes increases in both U-235's thermal production and U-235's thermal absorption, however, the former is faster than the latter. The increase in the variation in U-235's thermal production and that in U-235's thermal absorption is closely related to the fuel salt channel spacing. For a larger fuel salt channel spacing, the difference between U-235's thermal production and thermal absorption had no effect on the gap between the increment of U-235's thermal production and that of U-235's thermal production, and the increment in the variation in U-235's thermal production was still greater than that in U-235's thermal absorption, resulting in a positive thermal reproduction coefficient in the density coefficient. For a smaller fuel salt channel spacing, the difference between U-235's thermal production and U-235's thermal absorption was greater than the difference between their respective increments, and the increment in the variation in U-235's thermal production was smaller than that in U-235's thermal absorption, revealing a negative thermal reproduction coefficient in the density coefficient. With an increasing fuel salt volume fraction, the positive thermal reproduction coefficient caused by the density reduction effect gradually becomes the positive thermal reproduction coefficient caused by the spectrum softening effect. Therefore, negative feedback is attained. Figure 4c shows that with increasing fuel salt volume fraction, the positive thermal reproduction coefficient in the density coefficient first strengthens, then weakens, and becomes negative. The variation in the thermal reproduction coefficient in the density coefficient with assembly size is related to the moderated region. There was no significant difference in the thermal reproduction coefficient in the density coefficient between different assembly sizes in the over-moderated region. An increasing assembly size in the under-moderated region results in weakening negative feedback or strengthening positive feedback. When the assembly is near the optimal moderated region, the positive feedback caused by the softening spectrum effect gradually weakens as the assembly size increases. Overall, the thermal reproduction coefficient in the density coefficient contributes minimally (< 0.1 pcm/K) to the fuel salt density coefficient.

As the fuel salt temperature increases, its density decreases and the neutron spectrum softens. The thermal absorption of graphite increases owing to a softening neutron spectrum, and then the thermal absorption of graphite increases. The moderated regions affect the change in the thermal absorption of the fuel salt. In the over-moderated region, the thermal absorption of fuel salt decreases mainly owing to a reduction in fuel salt density, along with the thermal absorption of HMs and carrier salts. In this case, because the increase in thermal absorption of graphite is greater than the decrease in thermal absorption of the carrier salt as a result of a larger graphite volume fraction, the sum of thermal absorptions of graphite and carrier salt shows an increasing effect, and then the thermal utilization factor decreases. In the under-moderated region, the thermal absorption of HMs and that of carrier salt increase mainly owing to a softening neutron spectrum, however, the reduction in fuel salt density attenuates the increase rate of thermal absorption of HMs. Because the increase in the

thermal absorption of HMs is less than the sum of the thermal absorptions of the carrier salt and graphite, the thermal utilization factor decreases. In any case, the thermal utilization coefficient in the density coefficient, α_T^f(den), is always negative (Fig. 4d). Similarly, the magnitude of the thermal utilization coefficient in the density coefficient is closely related to the ratio of the sum of the thermal absorptions of the carrier salt and graphite to the thermal absorptions of all materials. As the fuel salt volume fraction increases for a constant assembly size, the ratio of the sum of the thermal absorptions of the carrier salt and graphite to the thermal absorptions of all materials gradually decreases with a decreasing graphite volume fraction, and then the negative thermal utilization coefficient in the density coefficient weakens. At a fixed fuel salt volume fraction, the difference in the thermal utilization coefficient in the density coefficient for different assembly sizes can be negligible.

The change in the fuel salt density coefficient with the fuel salt volume fraction and assembly size is depicted in Fig. 4e. Because the magnitude of the thermal reproduction coefficient is very small, the feedback and the magnitude of the density coefficient vary with the fuel salt volume fraction and assembly size, primarily owing to variations in the fast fission, resonance escape, and thermal utilization coefficients. First, in the over-moderated region, because the feedbacks of the fast fission and resonance escape coefficients are opposite and their magnitudes are close, the density coefficient exhibits a negative feedback owing to a more negative thermal utilization coefficient. Second, in the under-moderated region, the magnitude of the thermal utilization coefficient is small in comparison to the magnitudes of the fast fission and resonance escape coefficients, and the feedback and magnitude of the density coefficient are primarily determined by the latter two. Because the negative fast fission coefficient is weaker than the positive resonance escape coefficient, the feedback of the density coefficient is positive. Finally, the density coefficient is more sensitive to the fuel salt volume fraction than to the assembly size. With increasing fuel salt volume fraction, the negative density coefficient firstly decreases owing to a decreasing thermal utilization coefficient, then turns into an increasing positive density coefficient owing to an increasing positive resonance escape coefficient, and finally, the positive density coefficient decreases owing to an increasing negative fast fission coefficient.

3.4 Fuel salt temperature coefficient

The FSTC is a cumulative effect of the fuel salt Doppler and density coefficients, which can also be divided into four parts: the fast fission, resonance escape, thermal reproduction, and thermal utilization coefficients caused by the fuel salt temperature effect. Figure 5 shows the variations in the

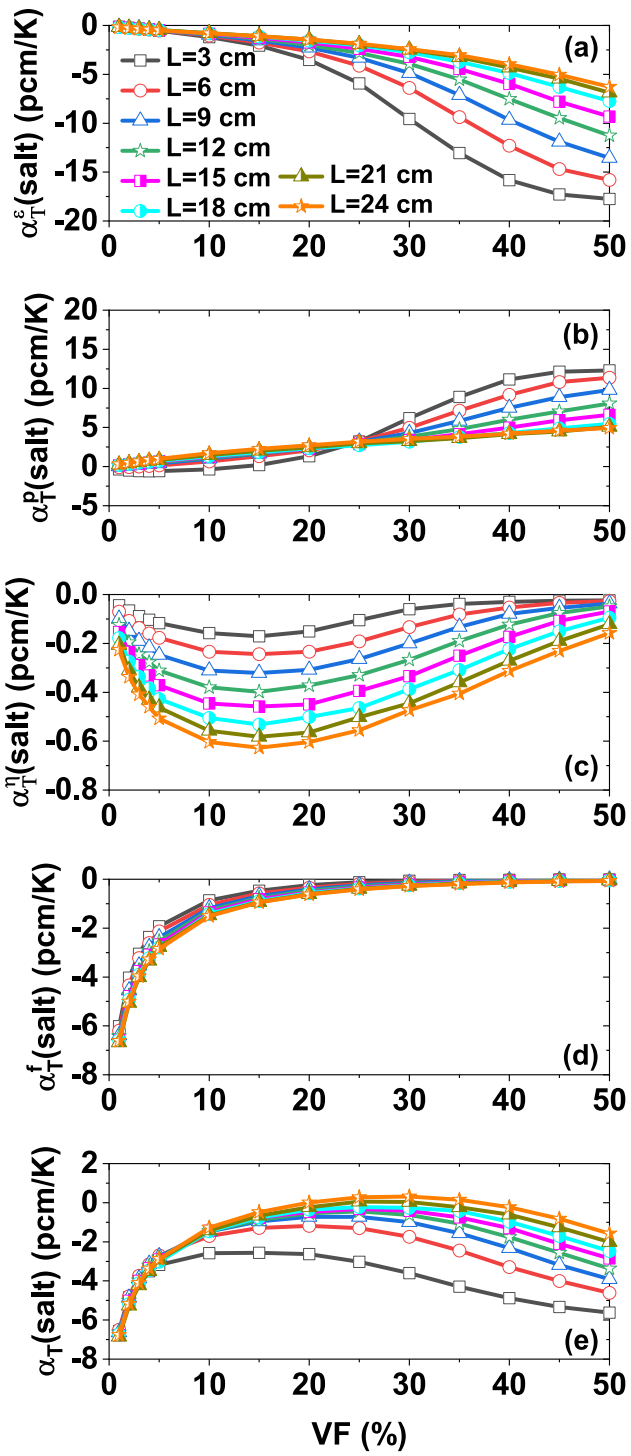

Fig. 5 (Color online) Variations in different reactivity coefficients caused by the fuel salt temperature effect as function of fuel salt volume fraction and assembly size. **a** α_T^ε(salt): fast fission coefficient in FSTC; **b** α_T^p(salt): resonance escape coefficient in FSTC; **c** α_T^η(salt): thermal reproduction coefficient in FSTC; **d** α_T^f(salt): thermal utilization coefficient in FSTC; and **e** α_T(salt): FSTC

four reactivity coefficients responsible for the behavior of FSTC.

The change in the fast fission factor caused by the temperature change of the fuel salt, α_T^{ε}(salt), is the sum of the fuel salt Doppler and density effects. Because the contribution of the positive Doppler effect is smaller than that of the negative fuel salt density effect, the fast fission coefficient in the FSTC is negative. The variation in the fast fission coefficient in the FSTC with the fuel salt volume fraction and assembly size is similar to that in the fuel salt density effect, and is displayed in Fig. 5a. When the neutron spectrum hardens (or softens) owing to variations in the fuel salt volume fraction or assembly size, the EALF increases (or decreases), and the magnitude of the fast fission coefficient in the FSTC increases (or decreases). That is, the magnitude of the fast fission coefficient in FSTC correlates positively with EALF.

The change in resonance escape probability caused by the temperature change in the fuel salt, α_T^{p}(salt), is also a sum of the fuel salt Doppler and density effects. For most combinations of fuel salt volume fraction and assembly size, the positive resonance escape coefficient caused by the fuel salt density effect is stronger than the negative resonance escape coefficient caused by the Doppler effect, resulting in a positive resonance escape coefficient in the FSTC. However, for an assembly with a smaller size (e.g., $L = 3$ cm) and smaller fuel salt volume fraction (e.g., $VF < 10\%$), the positive resonance escape coefficient caused by the fuel salt density effect is weaker than the negative resonance escape coefficient caused by the Doppler effect, resulting in a relatively weaker negative resonance escape coefficient in the FSTC. Figure 5b shows that, at a constant assembly size, the negative resonance escape coefficient in the FSTC becomes weaker and turns into a stronger positive feedback with increasing fuel salt volume fraction. This was mainly due to a gradual increase in the positive resonance escape coefficient caused by the fuel salt density effect. The magnitude of the resonance escape coefficient in the FSTC with a fixed fuel salt volume fraction is divided into two main regions based on the change in assembly size. In the over-moderated region, as the assembly size increases, the resonance escape coefficient in FSTC shifts from weaker negative feedback to stronger positive feedback owing to a weakening negative resonance escape coefficient caused by the Doppler effect. In the under-moderated region, a decreasing positive resonance escape coefficient caused by the fuel salt density effect causes the positive resonance escape coefficient in the FSTC to gradually decrease with increasing assembly size. In general, the larger the EALF, the greater the possibility of a positive resonance escape coefficient in the FSTC, and the stronger the positive resonance escape coefficient in the FSTC.

The thermal reproduction coefficient in the FSTC is also a sum of the fuel salt Doppler and density effects. Because the magnitude of the thermal reproduction coefficient caused by the fuel salt density effect is very small, the feedback and magnitude of the thermal reproduction coefficient in the FSTC are primarily determined by the Doppler effect. The thermal reproduction coefficient in the FSTC, α_T^{η}(salt), is a negative feedback. Figure 5c shows that the magnitude of the thermal reproduction coefficient in the FSTC first increases and then decreases as the fuel salt volume fraction increases, and shows a monotonic increasing tendency as the assembly size increases.

The thermal utilization coefficient in the FSTC is a product of the fuel salt Doppler and density effects. Because both the thermal utilization coefficient caused by the Doppler effect and that caused by the fuel salt density effect are negative, the thermal utilization coefficient in the FSTC, α_T^{f}(salt), is also negative. Figure 5d shows that, at a constant assembly size, the magnitude of the thermal utilization coefficient in the FSTC decreases, primarily owing to a decrease in the thermal utilization coefficient caused by the fuel salt density effect as the fuel salt volume fraction increases, while the fuel salt channel spacing decreases. For a constant fuel salt volume fraction, the magnitude of the thermal utilization coefficient in the FSTC increases slightly owing to a slightly increased thermal utilization coefficient caused by the Doppler effect, with an increase in the assembly size corresponding to a larger fuel salt channel spacing. In short, the negative thermal utilization coefficient in the FSTC is positively correlated with the fuel salt channel spacing. The larger the fuel salt channel spacing, the stronger the negative thermal utilization coefficient in the FSTC.

Figure 5e displays the change in the FSTC with the fuel salt volume fraction and assembly size. In the over-moderated region, the feedback and magnitude of the FSTC are primarily determined by the thermal utilization coefficient, and the FSTC is always negative. The magnitude of FSTC decreases as the fuel salt volume fraction increases, and there is little difference in magnitudes between different assembly sizes. In the under-moderated region, the feedback of the FSTC, mainly due to the fast fission, resonance escape, and thermal utilization coefficients, could be negative or positive. In this case, as the fuel salt volume fraction increases, the negative FSTC first decreases owing to a gradual weakening negative thermal utilization coefficient, and then increases owing to the enhancement rate of the fast fission coefficient being faster than that of the resonance escape coefficient. Furthermore, the magnitude of the FSTC declines with increasing assembly size, primarily owing to a decreasing negative fast fission coefficient. When the magnitude of the positive resonance escape coefficient is larger than the magnitude of the negative fast fission coefficient, FSTC presents a possibility of positive feedback, particularly

when the assembly size is ≥ 21 cm. It can be concluded that the variation in the FSTC with the fuel salt volume fraction is primarily caused by the fuel salt density effect, whereas the variation in the FSTC with the assembly size is primarily caused by the fuel salt Doppler effect.

3.5 Moderator temperature coefficient

As the graphite moderator temperature increases, the excitation of target nuclei (graphite nuclei) is more easily activated, the non-elastic scattering cross-section of target nuclei is larger, neutrons are more likely to obtain the sound energy of the scattered target nuclei [30], and the neutron spectrum moves toward the region where neutron energy is high. In addition, a harder neutron spectrum was revealed. The graphite MTC can also be divided into four parts: the fast fission, resonance escape, thermal reproduction, and thermal utilization coefficients, which are caused by the graphite temperature effect. Figure 6 depicts the variations in MTC and its four reactivity coefficients as a function of the fuel salt volume fraction and assembly size.

As the graphite moderator temperature increased, the neutron spectrum hardened, the fast neutron multiplication effect increased, and the fast fission factor increased. The fast fission coefficient in the MTC, α_T^{ε}(gra), is positive. The magnitude of the fast fission coefficient in the MTC is primarily determined by the difference between the variation in U-235's total production and that in U-235's thermal production, and is closely related to the fuel salt channel spacing. For a fixed assembly size, as the fuel salt volume fraction increases, the fuel salt channel spacing decreases, the neutron spectrum becomes harder, the proportion of thermal production in the total production for U-235 decreases, the difference between the variation in U-235's total production and that in U-235's thermal production increases, and the magnitude of the fast fission coefficient in the MTC increases (Fig. 6a). In the over-moderated region, for a constant fuel salt volume fraction, increasing the assembly size results in a hardening neutron spectrum. In this case, the larger the assembly size, the greater the parasitic thermal absorption of graphite, weakening the difference between the variation in U-235's total production and that in U-235's thermal production. Then, the magnitude of the fast fission coefficient in the MTC decreases slightly as the assembly size increases. In the under-moderated region, when the constant fuel salt volume fraction increases with assembly size, the fuel salt channel spacing increases, the neutron spectrum softens, the difference between the variation in U-235's total production and that in U-235's thermal production diminishes, and the fast fission coefficient in MTC weakens. In brief, the magnitude of the fast fission coefficient in the MTC is inversely proportional to the fuel salt channel spacing.

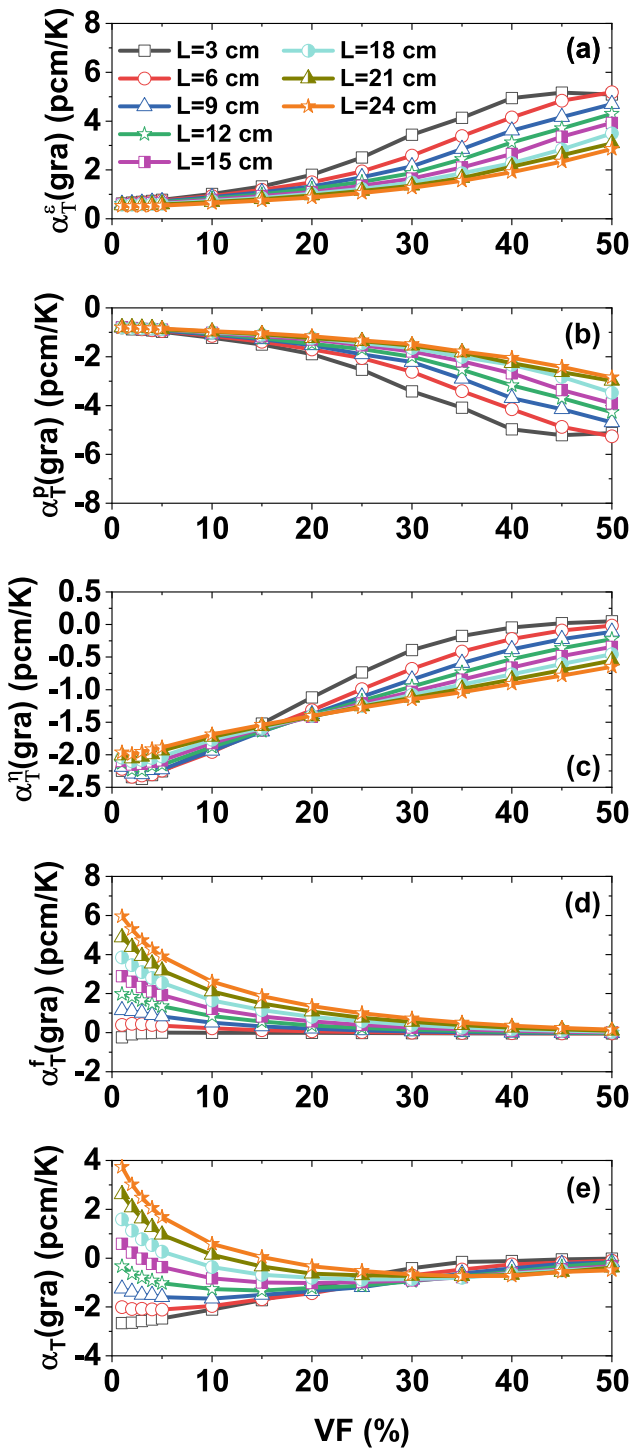

Fig. 6 (Color online) Variations in different reactivity coefficients caused by the graphite moderator temperature effect as function of fuel salt volume fraction and assembly size. **a** α_T^{ε}(gra): fast fission coefficient in MTC; **b** α_T^{p}(gra): resonance escape coefficient in MTC; **c** α_T^{η}(gra): thermal reproduction coefficient in MTC; **d** α_T^{f}(gra): thermal utilization coefficient in MTC; and **e** α_T(gra): MTC

A hardening neutron spectrum caused by an increasing graphite temperature results in a low microscopic absorption cross-section of graphite and a negative change in the thermal absorption of graphite. The change in the thermal absorption of the fuel salt is affected by the fuel salt channel spacing. When the fuel salt channel spacing is small, a harder neutron spectrum weakens the thermal absorption of fuel salt, resulting in a negative change in the thermal absorption of fuel salt, and the sum of the thermal absorptions of fuel salt and graphite is still negative. When the fuel salt channel spacing is large, the average distance traveled by neutrons between two collisions increases, allowing more neutrons to pass through the epi-thermal region and slowly transition to thermal neutrons. The change in the thermal absorption of the fuel salt was positive. In this case, the decrease in the thermal absorption of graphite exceeded the increase in the thermal absorption of the fuel salt owing to a larger graphite volume fraction. Hence, the sum of the thermal absorptions of the fuel salt and graphite remained negative, and a negative resonance escape coefficient in the MTC, α_T^p(gra) was revealed for all combinations of the fuel salt volume fraction and assembly size. It can be concluded from Fig. 6b that the magnitude of the resonance escape coefficient in the MTC as a function of the fuel salt volume fraction and assembly size is strongly related to the fuel salt channel spacing. If the fuel salt channel spacing decreases owing to a change in the fuel salt volume fraction or assembly size, the variation in the thermal absorption of the fuel salt gradually changes from positive to negative. This means that the net decrease in the thermal absorption of fuel salt grows increasingly larger. Meanwhile, the thermal absorption of graphite increases. Thus, the sum of the changes in the thermal absorptions of the fuel salt and graphite enhances the resonance escape coefficient in the MTC. In summary, the negative resonance escape coefficient in the MTC is generally inversely related to the fuel salt channel spacing.

For most combinations of fuel salt volume fraction and assembly size, an increasing graphite temperature causes a hardening neutron spectrum and a decrease in U-235's thermal production and thermal absorption. Although U-235's thermal production is larger than its thermal absorption, the former decreased faster than the latter. The variation in U-235's thermal production decreased more than that in U-235's thermal absorption, and the thermal reproduction factor decreased, causing a negative thermal reproduction coefficient in the MTC (α_T^η(gra)). However, there were two exceptions corresponding to very large fuel salt channel spacing and very small fuel salt channel spacing. When the fuel salt channel spacing was very small (e.g., $L = 3$ cm and $VF = 40\%$), a harder neutron spectrum caused a decrease in U-235's thermal production and thermal absorption, however, because graphite is relatively thin, the probability of thermal neutron generation is reduced. The values of thermal production and thermal absorption were similar, and the difference between them exceeded the difference between the decreases in U-235's thermal production and that of U-235's thermal absorption. Then, the variation in U-235's thermal production decreased less than that in U-235's thermal absorption, and thus the thermal reproduction factor decreased and a positive thermal reproduction coefficient in the MTC was presented. For extremely large fuel salt channel spacings (e.g., $L = 24$ cm and $VF = 1\%$), neutrons passing through thick graphite between two collisions with nuclear fuel had a higher chance of slowing down to thermal neutrons. U-235's thermal production and thermal absorption were increasing, however, the gap between them was wider than that between the increment in U-235's thermal production and thermal absorption. The variation in U-235's thermal production increased less than that in U-235's thermal absorption, the thermal reproduction factor decreased, and a negative thermal reproduction coefficient emerged in the MTC. According to the findings of the MTC [19], the magnitude of the thermal reproduction coefficient in the MTC was inversely related to the U-235 enrichment and the EALF, mainly due to the competition between the change of thermal production and that of thermal absorption. On the one hand, as shown in Figs. 2c and d, the required critical enrichment of U-235 first decreases and then increases, while EALF increases monotonously with increasing fuel salt volume fraction at a fixed assembly size. After superimposing the two effects, the magnitude of the thermal reproduction coefficient in the MTC with increasing fuel salt volume fraction for a constant assembly size was as follows (Fig. 6c): increased slowly at first, primarily due to a decreasing U-235 enrichment, and then decreased rapidly due to an increasing U-235 enrichment and an increasing EALF, and eventually turned to a positive feedback when fuel salt channel spacing was very small. The correlation between the thermal reproduction coefficient in the MTC and assembly size, was related to the moderated regions. As assembly gets closer to the over-moderated region, both U-235 enrichment and EALF increased as assembly size increased, and the magnitude of the thermal reproduction coefficient in the MTC decreased. In addition, as the assembly approached the under-moderated region, the values of U-235 enrichment and EALF decreased as the assembly size increased, and the magnitude of the thermal reproduction coefficient in the MTC increased.

As the temperature of the graphite moderator increased, the neutron spectrum hardened, causing the thermal absorption of graphite to decrease. The fuel salt channel spacing influenced the change in the thermal absorption of the fuel salt. The neutron spectrum effect dominated for smaller assembly sizes (e.g., $L = 3$ cm). The harder neutron spectrum reduced the thermal absorption of the fuel salt,

including the thermal absorptions of the HM and carrier salt. Because the graphite thickness for neutrons passing through between two adjacent fuel salt channels was relatively thin, the decrease in the thermal absorption of the HM was faster than that of the sum of the thermal absorptions of carrier salt and graphite, and the decrement in the variation in the thermal absorption of the HM was higher than that of the sum of the thermal absorptions of carrier salt and graphite; then, the thermal utilization factor decreased, and thus the thermal utilization coefficient in the MTC, α_T^f (gra), showed a negative feedback. For a larger assembly size (e.g., $L = 24$ cm), the feedback of the thermal utilization coefficient in the MTC was divided into two cases according to the moderated regions. On the one hand, when the assembly tended to the over-moderated region (e.g., $L = 24$ cm and $VF = 1\%$), the probability of a neutron slowing to a thermal neutron increased, along with the thermal absorption of fuel salt, increasing both the thermal absorption of the HM and that of the carrier salt. Because of the relatively thicker graphite moderator, the decrease in the thermal absorption of graphite was greater than the increase in the thermal absorption of the carrier salt. The sum of the thermal absorptions of the carrier salt and graphite had a decreasing trend, and then the increment of the variation of the thermal absorption of HMs and the decrement of the variation of the sum of the thermal absorptions of the carrier salt and graphite increased the thermal utilization factor, and thus the thermal utilization coefficient in the MTC was positive. On the other hand, when the assembly tended to the under-moderated region (e.g., $L = 24$ cm and $VF = 40\%$), a harder neutron spectrum decreased the thermal absorption of the HM and the sum of the thermal absorptions of the carrier salt and graphite. In this case, because the thermal absorption of HMs is considerably larger than the sum of the thermal absorptions of the carrier salt and graphite, the variation in the thermal absorption of HMs was larger than the variation in the thermal absorption of the carrier salt and graphite, which caused a positive thermal utilization coefficient in the MTC. Therefore, the thermal utilization coefficient in the MTC exhibited positive feedback for a larger fuel salt channel spacing or negative feedback for a smaller fuel salt channel spacing. Figure 6d shows that, as the fuel salt volume fraction increases for a fixed assembly size, the magnitude of the thermal utilization coefficient in the MTC decreases because the Maxwell spectrum is no longer visible. At a constant fuel salt volume fraction, as the assembly size increased, the fuel salt channel spacing increased, the graphite thickness through which fast neutrons were released from the fuel salt increased, and the change in the thermal absorption of graphite became more visible. The ratio of the sum of the thermal absorptions of carrier salt and graphite to the thermal absorptions of all materials was < 1.0, but grew larger, and then the thermal utilization coefficient in the MTC changed from less negative to more positive. When combined with the preceding analysis, the thermal utilization coefficient in the MTC was more negative for a smaller fuel salt channel spacing; otherwise, it was less negative or even positive.

Figure 6e depicts the change in the MTC with the fuel salt volume fraction and assembly size. Because the fast fission and resonance escape coefficients had opposite feedbacks but similar values, the feedback and magnitude of the MTC were primarily determined by the thermal reproduction and thermal utilization coefficients. The feedback of the MTC could be negative for an assembly with a smaller fuel salt channel spacing or positive for an assembly with a larger fuel salt channel spacing. The variation in the MTC with the fuel salt volume fraction can be divided into two regions: $L \leq 12$ cm and $L \geq 15$ cm. When the assembly size was ≤ 12 cm, because the magnitude of the thermal reproduction coefficient was larger than the thermal utilization coefficient, the MTC was negative. With an increase in fuel salt volume fraction, the magnitude of MTC first increased due to an increase in thermal reproduction coefficient, and then decreased because the decreasing rate of thermal reproduction coefficient was faster than that of thermal utilization coefficient. When the assembly size was ≥ 15 cm, the MTC changed from a decreasing positive feedback effect to an increasing negative feedback effect owing to a decreasing positive thermal utilization coefficient, and then to a decreasing negative feedback effect owing to a decreasing thermal reproduction coefficient. Additionally, the difference in the MTC between different assembly sizes was primarily caused by the thermal utilization coefficient. When the fuel salt volume fraction was $\leq 25\%$, the negative MTC weakened and gradually turned into stronger positive feedback as the positive thermal utilization coefficient grew stronger. When the fuel salt volume fraction was $> 25\%$, the negative MTC increased slightly with increasing assembly size, owing to a slightly enhanced thermal reproduction coefficient. Overall, the larger the fuel salt channel spacing, the more likely the MTC is to be positive.

3.6 Temperature coefficient of reactivity

Similarly, when the temperatures of the fuel salt and graphite in the assembly change, the fast fission, resonance escape, thermal reproduction, and thermal utilization coefficients contribute to the total temperature coefficient of reactivity. Their variations with the fuel salt volume fraction and assembly size are shown in Fig. 7.

The fast fission coefficient in TCR, α_T^ε(tot), shown in Fig. 7a, is the sum of the fuel salt temperature effect and graphite temperature effect. It can be divided into two regions by changing the fuel salt volume fraction and

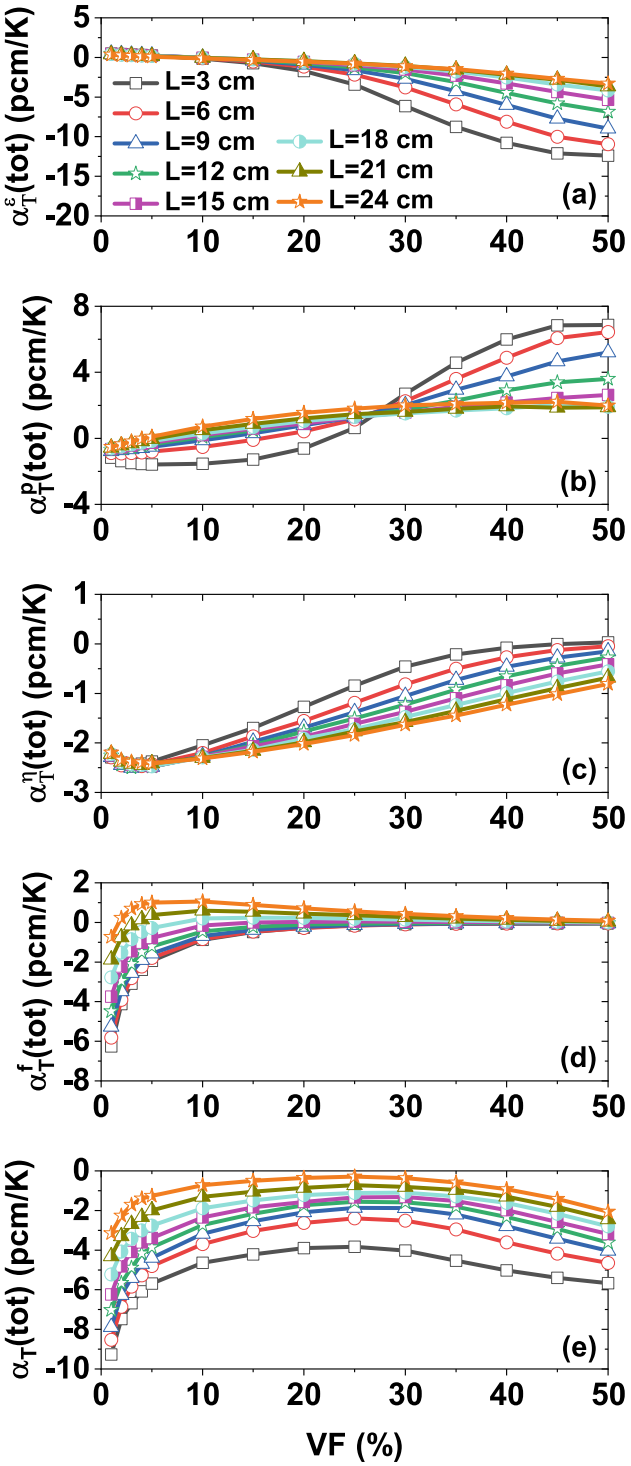

Fig. 7 (Color online) Variations in different reactivity coefficients caused by the total temperature effect as function of fuel salt volume fraction and assembly size. **a** α_T^{ε}(tot): fast fission coefficient in TCR; **b** α_T^{p}(tot): resonance escape coefficient in TCR; **c** α_T^{η}(tot): thermal reproduction coefficient in TCR; **d** α_T^{f}(tot): thermal utilization coefficient in TCR; and **e** α_T(tot): TCR

assembly size, corresponding to the over-moderated region and the under-moderated region. In the over-moderated region, the positive fast fission coefficient in MTC was stronger than the negative fast fission coefficient in FSTC, and the fast fission coefficient in TCR was positive. Owing to a change in the fast fission coefficient in MTC, the positive fast fission coefficient in TCR decreased with increasing fuel salt volume fraction or increasing assembly size. In the under-moderated region, the negative fast fission coefficient in the FSTC was stronger than the positive fast fission coefficient in the MTC, and the fast fission coefficient in the TCR was negative and strengthened with increasing fuel salt volume fraction or decreasing assembly size.

The resonance escape coefficient in TCR, α_T^{p}(tot), shown in Fig. 7b, is also a sum of the fuel salt temperature effect and graphite temperature effect. A combination of a smaller assembly size and a smaller fuel salt volume fraction increases the likelihood of the resonance escape coefficient in TCR being negative, owing to a negative resonance escape coefficient in MTC. With a fixed assembly size and increasing fuel salt volume fraction, the negative resonance escape coefficient in the TCR decreased gradually and then became increasing positive feedback. When the fuel salt volume fraction was < 25%, the negative resonance escape coefficient in TCR gradually decreased and became increasing positive feedback as the assembly size increased. When the fuel salt volume fraction was ≥25%, the positive resonance escape coefficient in TCR decreased with increasing assembly size.

The thermal reproduction coefficient in TCR, α_T^{η}(tot), shown in Fig. 7c, is the sum of the thermal reproduction coefficients in FSTC and MTC. Because the thermal reproduction coefficient in FSTC was markedly weaker than that in MTC, the feedback and magnitude of the thermal reproduction coefficient in TCR were primarily determined by the latter. The feedback of the thermal reproduction coefficient in TCR was negative. The variation in the thermal reproduction coefficient in TCR with fuel salt volume fraction and assembly size was similar to that in MTC. When the fuel salt volume fraction increased at a constant assembly size, the negative thermal reproduction coefficient in TCR first increased and then decreased. When the assembly size increased for a constant fuel salt volume fraction, the thermal reproduction coefficient in TCR either weakened in the over-moderated region or strengthened in the under-moderated region.

As a sum of the thermal utilization coefficients in FSTC and MTC, the thermal utilization coefficient in TCR, α_T^{f}(tot), shown in Fig. 7d, could be negative or positive. When the assembly size was ≤ 12 cm, the negative thermal utilization coefficient in the FSTC had a greater magnitude than the positive thermal utilization coefficient in the MTC. In this case, the thermal utilization coefficient in TCR was negative,

and its magnitude decreased with increasing fuel salt volume fraction owing to a decreasing thermal utilization coefficient in FSTC. Simultaneously, the magnitude of the thermal utilization coefficient in TCR decreased with increasing assembly size because the thermal utilization coefficient in the MTC changed from less negative to strongly positive. When the assembly size was ≥15 cm, as the fuel salt volume fraction increased for a fixed assembly size, the negative thermal utilization coefficient in TCR decreased and turned into an increasing positive feedback, owing to a decreasing negative thermal utilization coefficient in FSTC, and then the positive thermal utilization coefficient in TCR decreased due to a decreasing thermal utilization coefficient in the MTC. As the assembly size increased for a constant fuel salt volume fraction, the negative thermal utilization coefficient in TCR weakened and then became a more strongly positive feedback. In other words, an assembly with a smaller fuel salt channel spacing presents higher probabilities of presenting a more negative thermal utilization coefficient in the TCR.

Figure 7e depicts the change in TCR with the fuel salt volume fraction and assembly size. The TCR was negative because the sum of the negative fast fission, negative thermal reproduction, and negative thermal utilization coefficients was greater than the positive resonance escape coefficient. As the fuel salt volume fraction increased for a constant assembly size, the magnitude of TCR varied with fuel salt volume fraction in three cases with 5% and 25% as the cut-off points. When the fuel salt volume fraction was ≤ 5%, the magnitude of TCR decreased rapidly, primarily owing to the rapid decrease in the negative thermal utilization coefficient, particularly that caused by the fuel salt density effect. When the fuel salt volume fraction was between 5% and 25%, the magnitude of TCR decreased slowly, because the change rate of the sum of the resonance escape, thermal reproduction, and thermal utilization coefficients was faster than that of the negative fast fission coefficient. When the fuel salt volume fraction was > 25%, the TCR strengthened slowly, because the growth rate of the negative fast fission coefficient was greater than that of the sum of the other three reactivity coefficients. For a constant fuel salt volume fraction, the change in TCR with assembly size was primarily due to a balance between the fast fission coefficient and thermal utilization coefficient. As the assembly size increased, the decrease rate of the negative fast fission coefficient was faster than that of the negative thermal utilization coefficient, therefore, TCR weakened gradually. Finally, the magnitude of TCR first decreased and then increased with increasing fuel salt volume fraction, and it decreased monotonously with increasing assembly size. Notably, the contributions of the fast fission, resonance escape, and thermal reproduction coefficients in TCR were primarily from the fuel salt density effect, whereas the contribution of the thermal utilization coefficient in TCR was mainly from the fuel salt density and graphite temperature effects. In addition, the variation in TCR with fuel salt volume fraction mainly came from the fuel salt density effect, whereas the variation in TCR with assembly size mainly came from the graphite temperature effect.

4 Conclusion

Based on a graphite-moderated and low-enriched uranium-fueled fuel salt assembly, the four-factor formula was used to evaluate the effects of geometric parameters, including fuel salt volume ratio and assembly size, on TCR. When the assembly temperature increased, the fuel salt Doppler effect and the graphite moderator temperature effect hardened the neutron spectrum, while the fuel salt density effect softened it, affecting both the feedback and the magnitude of TCR.

Positive fast fission and negative resonance escape coefficients were observed in the fuel salt Doppler and graphite moderator temperature coefficients. Negative fast fission and positive resonance escape coefficients were revealed in the fuel salt density coefficient. The feedback of the thermal reproduction coefficient could be positive or negative in all reactivity coefficients. The feedback of the thermal utilization coefficient in the Doppler coefficient and density coefficient was negative, whereas that in the graphite moderator temperature coefficient could be negative or positive. Furthermore, the Maxwell, resonant neutron, and full neutron spectrums mainly affected the graphite temperature, fuel salt Doppler, and fuel salt density effects, respectively. The full neutron spectrum had the greatest influence on the changes in the fast fission and resonance escape factors. From low to high, the magnitudes of the fast fission coefficients were α_T^{ε}(gra), α_T^{ε}(dop), and α_T^{ε}(den). Similarly, the magnitudes of the resonance escape coefficients were also α_T^{p}(gra), α_T^{p}(dop), and α_T^{p}(den) from low to high. Because the thermal neutron spectrum had the greatest influence on the thermal reproduction factor, the magnitudes of the thermal reproduction coefficients were α_T^{η}(den), α_T^{η}(dop), and α_T^{η}(gra) from low to high. The thermal utilization factor was a relatively complex variable, with magnitudes ranging from low to high for α_T^{f}(dop), α_T^{f}(gra), and α_T^{f}(den).

The FSTC is a combined effect of the fuel salt Doppler and fuel salt density coefficients. The fuel salt Doppler coefficient was always negative. The fuel salt density coefficient could be either negative in the over-moderated region owing to its negative thermal utilization coefficient or positive in the under-moderated region owing to its positive resonance escape coefficient. The magnitude of the FSTC first decreased and then increased as the fuel salt volume fraction increased. This was primarily because the fuel salt density coefficient shifted from decreasing negative feedback to

increasing positive feedback and then decreasing positive feedback. The magnitude of the FSTC decreased monotonously as the assembly size increased, mainly owing to a monotonously decreasing Doppler coefficient.

The MTC can be negative or positive depending on the fuel salt channel spacing. The smaller the fuel salt channel spacing, the more likely the MTC is to be negative, owing to a negative thermal reproduction coefficient. Because of a gradually weakened thermal reproduction coefficient and thermal utilization coefficient, the magnitude of the MTC decreased as the fuel salt volume fraction increased. As assembly size increased, MTC transitioned from weakened negative feedback to enhanced positive feedback as a result of the change in the thermal utilization coefficient, and when the fuel salt volume fraction was relatively lower, the influence of fuel salt channel spacing on MTC was more visible.

At the assembly level, the total temperature coefficient of reactivity was negative, regardless of whether the region was over-moderated or under-moderated, which met the safety requirements of reactor operation. The magnitude of the TCR in the under-moderated region was smaller than that in the over-moderated region, and the power change rate was comparatively slower, which could be conducive to reactor safety. The MTC was more likely to be negative in the under-moderated region, particularly for an assembly with a smaller fuel salt channel spacing. Consequently, an assembly with a smaller fuel salt channel spacing in the under-moderated region was preferred to achieve a reasonably negative TCR and negative MTC. Thermal-hydraulic and transient analyses were also required to assess the reasonableness of the magnitude of TCR to ensure the intrinsic safety of a liquid-fueled MSR. Future studies will include the following items: friction pressure decrease, heat conduction ability of graphite, consequences of abnormal reactivity introduced into it, and blockage of fuel salt. In addition to geometrical parameters, fuel salt composition was another crucial factor influencing the TCR for a thermal MSR, particularly when fuel salt reprocessing and online refueling were used. To fully understand the mechanism of TCR for thermal MSR, more research is required to address how TCR is affected by both geometric parameters and fuel salt composition.

Author Contributions All authors contributed to the study conception and design. Material preparation, data collection and analysis were performed by Xiao-Xiao Li, De-Yang Cui and Jin-Gen Chen. The first draft of the manuscript was written by Xiao-Xiao Li and all authors commented on previous versions of the manuscript. All authors read and approved the final manuscript.

Data availability statement The data that support the findings of this study are openly available in Science Data Bank at https://doi.org/10.57760/sciencedb.j00186.00069 and https://cstr.cn/31253.11.sciencedb.j00186.00069.

Conflict of interest Xiang-Zhou Cai is an editorial board member for Nuclear Science and Techniques and was not involved in the editorial review, or the decision to publish this article. All authors declare that there are no competing interests.

References

1. V.I. Victor, Molten salt reactors. Encyclopedia. Nucl Energy **1**, 553–568 (2021). https://doi.org/10.1016/B978-0-12-409548-9.12208-0
2. N. Taheranpour, A. Talaei, Development of practical method using a Monte Carlo code for evaluation of optimum fuel pitch in a typical VVER-1000 core. Ann. Nucl. Energy **54**, 129–133 (2013). https://doi.org/10.1016/j.anucene.2012.10.029
3. F. Qayyum, M.R. Ali, A. Zahur et al., Improvements in methodology to determine feedback reactivity coefficients. Nucl. Sci. Tech. **30**, 63 (2019). https://doi.org/10.1007/s41365-019-0588-0
4. S.H. Yu, Y.F. Liu, P. Yang et al., Neutronics analysis for MSR cell with different fuel salt channel geometries. Nucl. Sci. Tech. **32**(1), 9 (2019). https://doi.org/10.1007/s41365-020-00844-0
5. A. Rykhlevskii, J.W. Bae, K.D. Huff, Modeling and simulation of online reprocessing in the thorium-fueled molten salt breeder reactor. Ann. Nucl. Energy **128**, 366–379 (2019). https://doi.org/10.1016/j.anucene.2019.01.030
6. D.Y. Cui, X.X. Li, Y. Dai et al., An improved core design of a 50 kWth heat pipe cooled micro Molten salt reactor (micro-MSR). Prog. Nucl. Energy **151**, 104326 (2022). https://doi.org/10.1016/j.pnucene.2022.104326
7. D.Y. Cui, S.P. Xia, X.X. Li et al., Transition toward thorium fuel cycle in a molten salt reactor by using plutonium. Nucl. Sci. Tech. **28**(10), 152 (2017). https://doi.org/10.1007/s41365-017-0303-y
8. G.C. Li, P. Cong, C.G. Yu et al., Optimization of Th-U fuel breeding based on a single-fluid double-zone thorium molten salt reactor. Prog. Nucl. Energy **108**, 144–151 (2018). https://doi.org/10.1016/j.pnucene.2018.04.017
9. C.Y. Zou, C.G. Yu, J.H. Wu et al., Ameliorating the positive temperature feedback coefficient for an MSR fueled with transuranic elements. Ann. Nucl. Energy **160**(15), 108325 (2021). https://doi.org/10.1016/j.anucene.2021.108325
10. J.H. Wu, J.G. Chen, X.Z. Kang et al., A novel concept for a molten salt reactor moderated by heavy water. Ann. Nucl. Energy **132**, 391–403 (2019). https://doi.org/10.1016/j.anucene.2019.04.043
11. L. Mathieu, D. Heuer, R. Brissot et al., The thorium molten salt reactor: moving on from the MSBR. Prog. Nucl. Energy **48**(7), 664–679 (2006). https://doi.org/10.1016/j.pnucene.2006.07.005
12. S.Q. Jaradat, A.B. Alajo, Studies on the liquid fluoride thorium reactor: comparative neutronics analysis of MCNP6 code with SRAC95 reactor analysis code based on FUJI-U3-(0). Nucl. Eng. Des. **314**, 251–255 (2017). https://doi.org/10.1016/j.nucengdes.2017.02.013

13. L. Mathieu, D. Heuer, E. Merle-Lucotte et al., Possible configurations for the thorium molten salt reactor and advantages of the fast nonmoderated version. Nucl. Sci. Eng. **161**(1), 78–89 (2009). https://doi.org/10.13182/NSE07-49
14. J. Křepel, B. Hombourger, C. Fiorina et al., Fuel cycle advantages and dynamics features of liquid fueled MSR. Ann. Nucl. Energy **64**, 380–397 (2014). https://doi.org/10.1016/j.anucene.2013.08.007
15. C.Y. Zou, X.Z. Cai, D.Z. Jiang et al., Optimization of temperature coefficient and breeding ratio for a graphite-moderated molten salt reactor. Nucl. Eng. Des. **281**, 114–120 (2015). https://doi.org/10.1016/j.nucengdes.2014.11.022
16. C.N.A.C.Z. Bahri, W.M. Al-Areqi, M.I.F.M. Ruf et al., Characteristic of molten fluoride salt system LiF-BeF_2 (Flibe) and LiF-NaF-KF (Flinak) as coolant and fuel carrier in molten salt reactor (MSR). AIP Conf. Proc. **1799**, 040008 (2017). https://doi.org/10.1063/1.4972932
17. B. Hombourger, J. Křepel, A. Pautz, Breed-and-burn fuel cycle in molten salt reactors. EPJ Nucl. Sci. Technol. **5**, 15 (2019). https://doi.org/10.1051/epjn/2019026
18. X.X. Li, Y.W. Ma, C.G. Yu et al., Effects of fuel salt composition on fuel salt temperature coefficient (FSTC) for an undermoderated molten salt reactor (MSR). Nucl. Sci. Tech. **29**(8), 110 (2018). https://doi.org/10.1007/s41365-018-0458-1
19. X.X. Li, D.Y. Cui, Y.W. Ma et al., Influence of ^{235}U enrichment on the moderator temperature coefficient of reactivity in a graphite-moderated molten salt reactor. Nucl. Sci. Tech. **30**(11), 166 (2019). https://doi.org/10.1007/s41365-019-0694-z
20. M.L. Tan, G.F. Zhu, Y. Zou et al., Research on the effect of the heavy nuclei amount on the temperature reactivity coefficient in a small modular molten salt reactor. Nucl. Sci. Tech. **30**(9), 140 (2019). https://doi.org/10.1007/s41365-019-0666-3
21. B.A. Hombourger, J. Křepel, K. Mikityuk et al., Parametric lattice study of a graphite-moderated Molten Salt Reactor. J. Nucl. Eng. Radiat. Sci. **1**(1), 011009 (2015). https://doi.org/10.1115/1.4026401
22. J. Křepel, E. Losa, Self-sustaining breeding in advanced reactors: characterization of selected reactors. Encycl. Nucl. Energy **64**, 801–819 (2021). https://doi.org/10.1016/B978-0-12-819725-7.00123-9
23. Y. Zhu, A.I. Hawari, Thermal neutron scattering cross section of liquid FLiBe. Prog. Nucl. Energy **101**(Part C), 468–475 (2017). https://doi.org/10.1016/j.pnucene.2017.03.028
24. Y.F. Liu, W.J. Li, R. Yan et al., Effect of FLiBe thermal neutron scattering on reactivity of molten salt reactor. Euro. Phys. J. Conf. **239**, 4008 (2020). https://doi.org/10.1051/epjconf/202023914008
25. C.W. Lau, C. Demaziere, H. Nylen et al., Improvement of LWR thermal margins by introducing thorium. Prog. Nucl. Energy **61**, 48–56 (2012). https://doi.org/10.1016/j.pnucene.2012.07.004
26. R.L. Murray, K.E. Holbert, Nuclear energy (eighth edition) chapter 16-neutron chain reactions. Nucl. Energy **291**, 305 (2020). https://doi.org/10.1016/B978-0-12-812881-7.00016-2
27. X. Wang, R. Macian-Juan, Steady-state reactor physics of the dual fluid reactor concept. Int. J. Energy Res. **42**, 4313–4334 (2018). https://doi.org/10.1002/er.4171
28. E.E. Bende, Temperature reactivity effects in pebbles of a high-temperature reactor fueled with reactor-grade plutonium. Nucl. Technol. **131**(3), 279–296 (2000). https://doi.org/10.13182/NT00-A3117
29. M. Dallas, W. Alexander, C. Ondřej, Lattice optimization for graphite moderated molten salt reactors using low-enriched uranium fuel. Ann. Nucl. Energy **110**, 1–10 (2017). https://doi.org/10.1016/j.anucene.2017.06.015
30. I.I. Al-Qasir, Y.Q. Cheng, J.Y.Y. Lin et al., Neutron thermalization in nuclear graphite: a modern story of a classic moderator. Ann. Nucl. Energy **161**, 108437 (2021). https://doi.org/10.1016/j.anucene.2021.108437